ADVANCED OPTICAL MATERIALS

Supporting Information

for *Adv. Optical Mater.,* DOI: 10.1002/adom.202001467

Mode Engineering in Large Arrays of Coupled Plasmonic–Dielectric Nanoantennas

Mazhar E. Nasir, Alexey V. Krasavin, R. Margoth Córdova-Castro, Cillian P. T. McPolin, Jean-Sebastien G. Bouillard, Pan Wang, and Anatoly V. Zayats*

Supporting Information

Mode Engineering in Large Arrays of Coupled Plasmonic-Dielectric Nanoantennas

Mazhar E. Nasir[1,], Alexey V. Krasavin[1], R. Margoth Córdova-Castro[1], Cillian P. T. McPolin[1], Jean-Sebastien G. Bouillard[2,3], Pan Wang[1], and Anatoly V. Zayats[1]*

[1] *Department of Physics and London Centre for Nanotechnology, King's College London, Strand, London WC2R 2LS, UK*

[2] *Department of Physics and Mathematics, University of Hull, Hull HU6 7RX, UK*

[3] *G. W. Gray Centre for Advanced Materials, University of Hull, UK*

**corresponding author: mazhar.nasir@kcl.ac.uk*

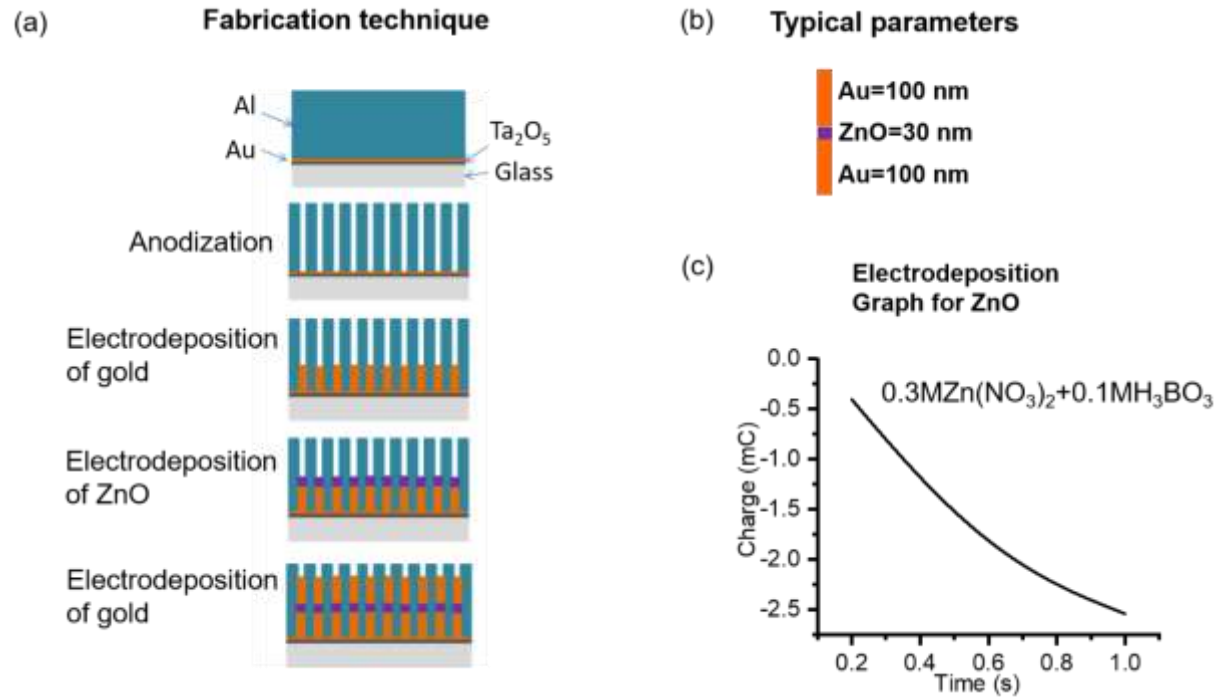

Figure S1. (a) Fabrication process flow for Au-ZnO-Au split-rod metamaterials. (b) Typical parmeters of the nano-antenna components. (c) Time-charge graph for the ZnO electro-deposition.

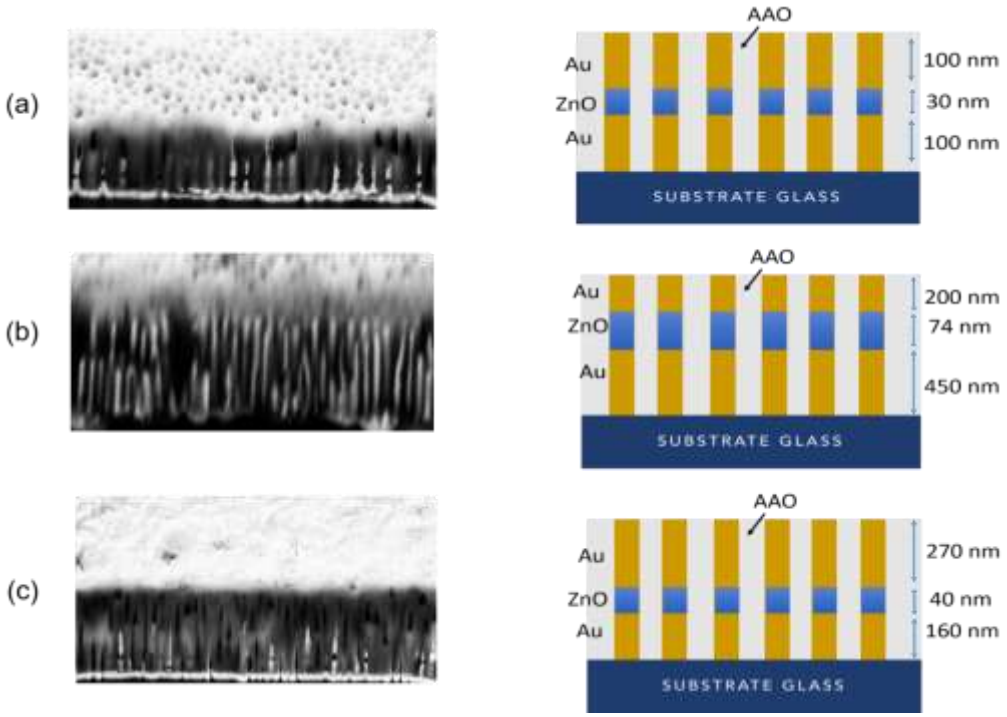

Figure S2. SEM cross-section images of samples A, B and C showing different lengths of Au and ZnO segments of the nano-antenna. The lengths of the segments are controlled by the electrodeposition times.

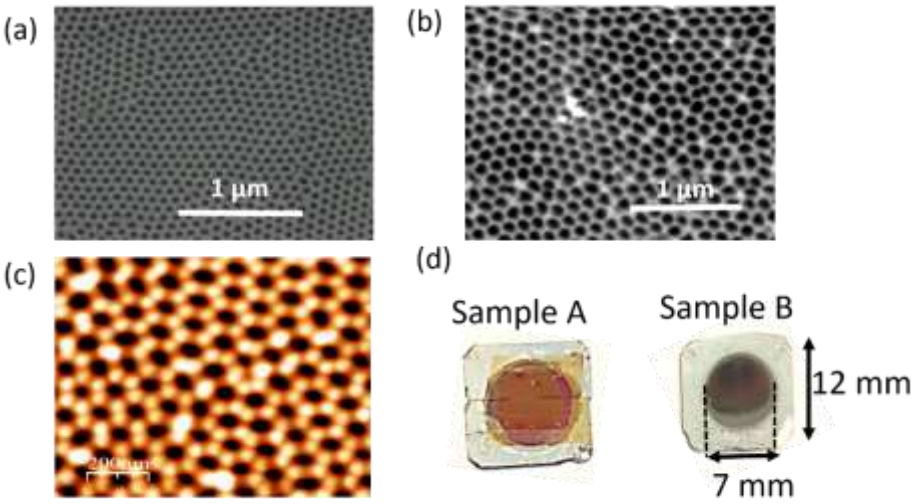

Figure S3. (a,b) SEM images of the porous alumina templates which define the diameter and spacing of the split-rod nanoantennas: (a) diameter 50 nm and period 100 nm, (b) diameter 100 nm and period 150 nm. (c) AFM image of porous alumina template with pore diameter 40 nm and period 100 nm. (d) Photographs of the samples.

(a)

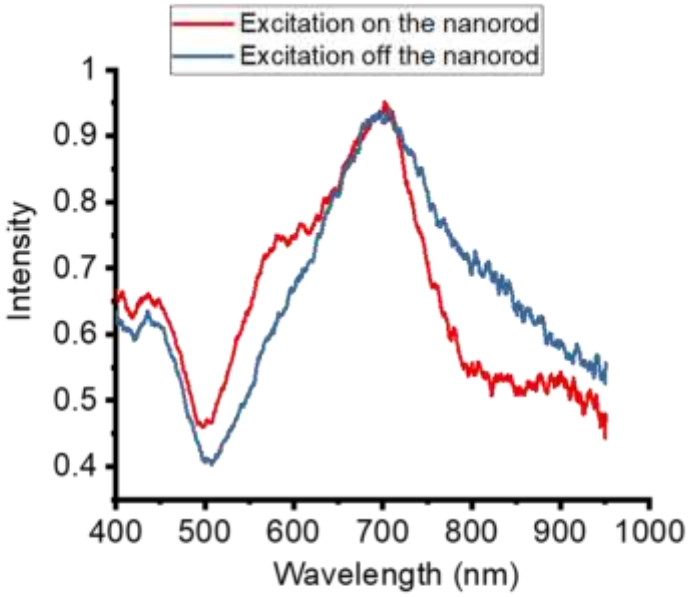

(b)

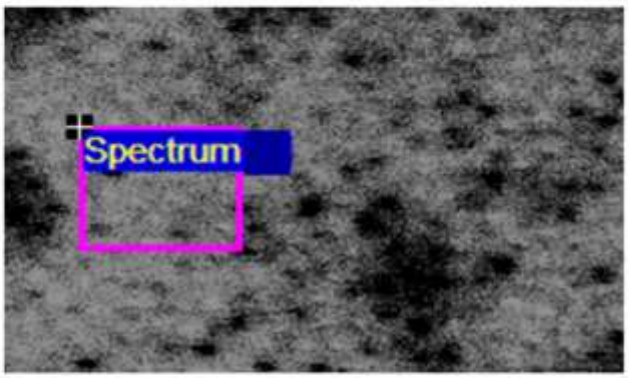

Elements	Weight %	Atomic %
O	49.40	75.40
Al	23.32	21.11
Zn	0.43	0.16
Au	26.86	3.33

Figure S4: (a) Cathodoluminescence spectra of sample A measured with the exciting electron beam focused on and off the individual nanorod in the array. ZnO related emission is observed at around 580 nm when excited on the nanorod. (b) EDX analysis of sample B showing percentage of Zn and O present. Zn comes from the ZnO compound while oxygen contribution comes from both the alumina and ZnO.

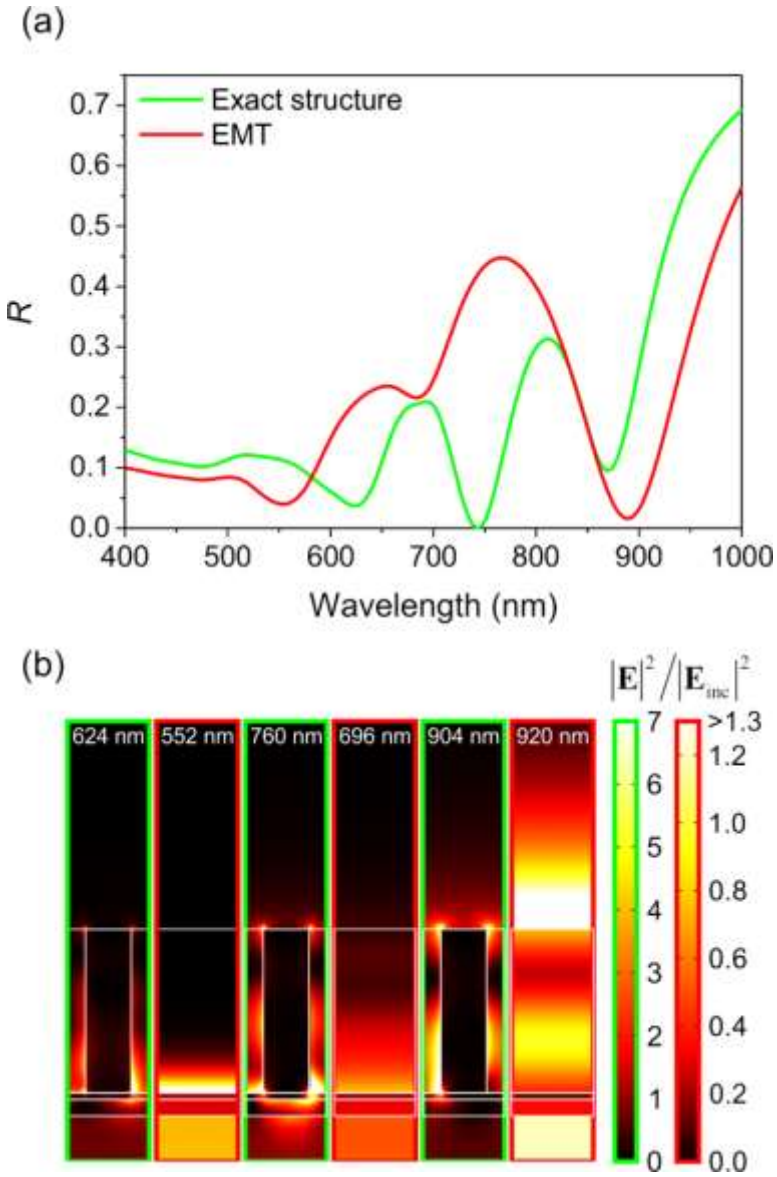

Figure S5. (a) Reflectivity of the metamaterial layer without a gap obtained using numerical modelling of the exact nano-antenna structure (green line) and the metamaterial heterostructure approximated using the EMT (red line), under illumination of the split-rod metamaterial with *p*-polarized light at 70°. (b) Electric field intensity profiles of the guided modes corresponding to the minima in (a).

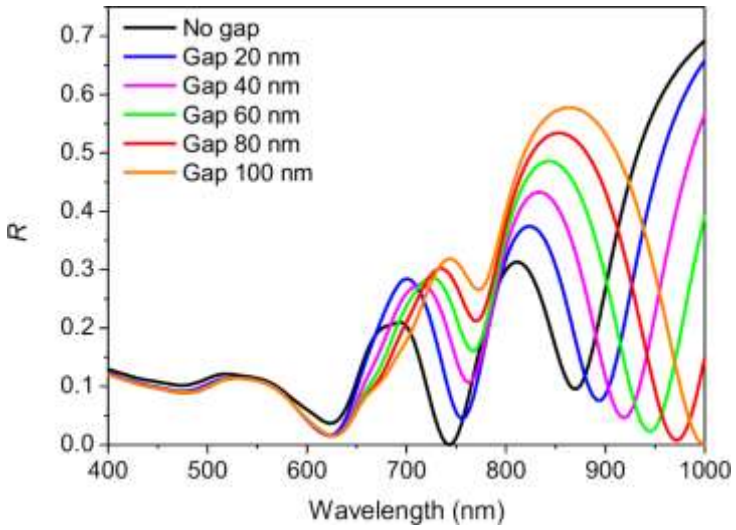

Figure S6. Spectral dependence of reflection from the split-rod metamaterial layer as a function of the gap width, under illumination of the split-rod metamaterial with *p*-polarized light at 70°.

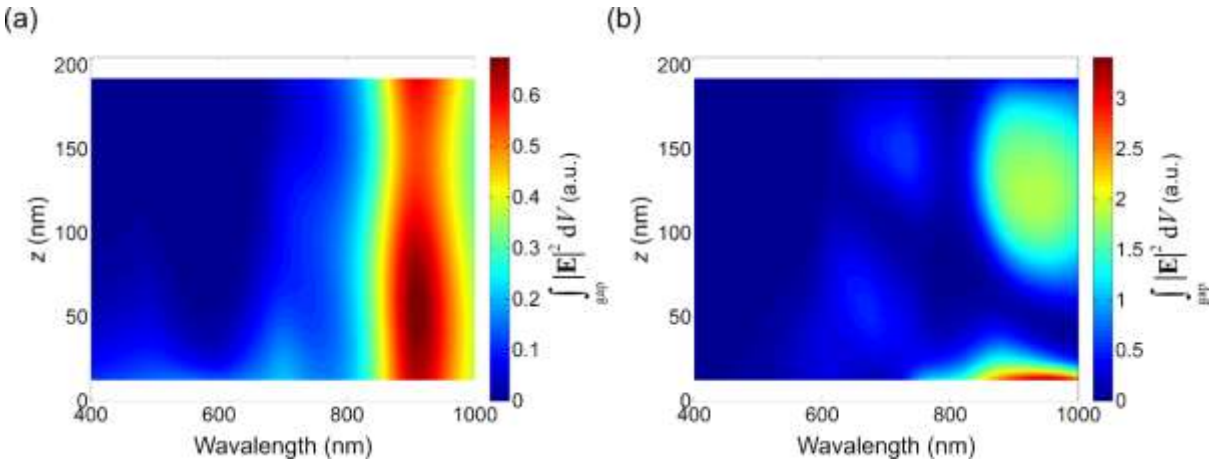

Figure S7. Electric field intensity integrated over the metamaterial gap layer obtained (a) in the EMT approximation and (b) in the corresponding region with the exact nano-antenna structure, under illumination of the split-rod metamaterial with *p*-polarized light at 70°.

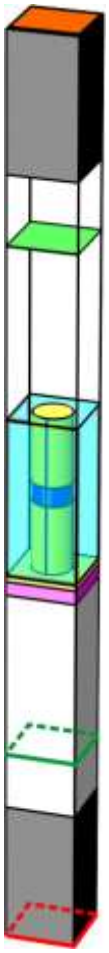

Figure S8. Simulation model presenting a metamaterial unit cell with the geometrical parameters corresponding to Sample A. Domains: (yellow) Au, (blue) ZnO, (semi-transparent cyan) Al_2O_3, (magenta) Ta_2O_5, (light grey) SiO_2, (transparent) air, (dark grey) PMLs; boundaries: (red) scattering boundary with plane wave excitation, (orange) scattering boundary, (bright green) integration boundary for transmission, (dark green) integration boundary for reflection; periodic boundary conditions applied to all side boundaries.